

July 15, 2017

# Top-Higgs Yukawa Coupling Measurement at a Linear $e^+e^-$ Collider

AURELIO JUSTE<sup>1</sup>, GONZALO MERINO<sup>2</sup>

1) Fermi National Accelerator Laboratory,  
P.O. Box 500, MS 357,  
Batavia, IL 60510,  
Phone: 1 (630) 840-6565 Fax: 1 (630) 840-8481  
e-mail: juste@fnal.gov

2) Institut de Física d'Altes Energies,  
Universitat Autònoma de Barcelona,  
E-08193 Bellaterra (Barcelona), Spain.  
Phone: 34 (93) 581-2846 Fax: 34 (93) 581-1938  
e-mail: merino@ifae.es

## Abstract

A feasibility study of the measurement of the top-Higgs Yukawa coupling at a future linear  $e^+e^-$  collider operating at  $\sqrt{s} = 800$  GeV is presented. As compared to previous existing studies, much effort has been put in a “realistic simulation” by including irreducible+reducible backgrounds, realistic detector effects and reconstruction procedures and finally, a multivariate analysis. Both hadronic and semileptonic decay channels have been considered.

# 1 Introduction

The theory of electroweak interactions has been successfully tested so far to an extremely high degree of accuracy. However, one of its key elements, the Higgs mechanism, remains to be tested experimentally. It is through the interaction with the ground state Higgs field that the fundamental particles acquire mass, which in turn sets the scale of the coupling with the Higgs boson. Once the Higgs boson is found (if ever), all its properties have to be accurately measured: mass, width, etc, and indeed its couplings to bosons and fermions. The couplings to the  $Z$  and  $W$  gauge bosons can be measured from the Higgstrahlung process:  $Z \rightarrow ZH$  [1] and the fusion processes:  $WW, ZZ \rightarrow H$  [2]. On the other hand, the top quark provides a unique opportunity to measure the Higgs Yukawa coupling to fermions. Being proportional to the fermion mass,

$$g_{ffH} = \frac{m_f}{v}, \quad (1.1)$$

with  $v = (\sqrt{2} G_F)^{-1/2} \simeq 246$  GeV, the top-Higgs Yukawa coupling is the largest among the different fermions:  $g_{ttH}^2 \simeq 0.5$  to be compared for instance with  $g_{bbH}^2 \simeq 4 \times 10^{-4}$ .

The process  $e^+e^- \rightarrow t\bar{t}H$  provides a chance for a direct measurement of the top-Higgs Yukawa coupling [8, 9] in the “Light Higgs Scenario” ( $M_H \leq 2m_t$ ), which seems to be favored by the present precision electroweak data ( $M_H = 76_{-47}^{+85}$  GeV as reported in [5]). On the other hand, the current limit from direct search at LEP2 is  $M_H > 95.2$  GeV at 95% CL [6]. The total cross-section depends sensitively on the top-Higgs Yukawa coupling, which can thus be inferred from the comparison of the measured total cross-section with the theoretical expectation as a function of  $g_{ttH}$ . This measurement of  $g_{ttH}$  is direct as compared to the indirect determination via its effect in the interquark potential near the  $t\bar{t}$  production threshold, which affects some threshold observables [7].

In this study we are going to assume that the MSM Higgs boson has already been discovered and its mass measured to be  $M_H = 120$  GeV. For  $M_H = 120$  GeV, the Higgs decays dominantly to  $b\bar{b}$  ( $\text{BR}(H \rightarrow b\bar{b}) \simeq 77\%$ ), and assuming  $\text{BR}(t \rightarrow Wb) = 100\%$ , this leads to multi-jet event topologies involving 4 b-jets in the final state. Therefore, one of the crucial experimental aspects will be flavor tagging.

Previous studies on the feasibility of this measurement have already been performed [3], but they were assuming a too simplistic simulation of detector effects (in particular b-tagging, which is critical here) and/or considering too few background processes. More complete studies have recently been presented [4].

## 2 Theoretical Scenario

At lowest order there are 5 diagrams contributing to this process, as shown in Fig. 1. The dominant contribution comes from  $\gamma$ -exchange with the  $H$  being radiated off the  $t$  or the  $\bar{t}$ . The diagram in which the  $H$  is radiated off the  $Z$  constitutes just a small correction, so that the total cross-section is to a good approximation  $\propto g_{ttH}^2$  (see Fig. 2a).

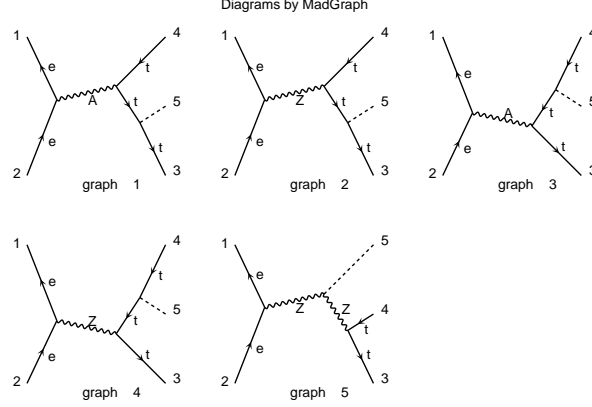


Figure 1: Tree level diagrams contributing to the process  $t\bar{t}H$ .

As it can be observed in Fig. 2a, the total cross-section decreases at low  $\sqrt{s}$  due to phase-space restrictions and at high  $\sqrt{s}$  due to unitarity. Radiative effects in the initial state (initial state radiation and beamstrahlung) become increasingly important for high  $\sqrt{s}$  and significantly distort the  $t\bar{t}H$  lineshape, as shown in Fig. 2b. The main effect is to shift the maximum of the cross-section towards higher  $\sqrt{s}$ , which for  $M_H = 120$  GeV is around  $\sqrt{s} \simeq 800$  GeV. Initial state radiation turns out to be the dominant radiative process in order to decrease the sensitivity of the total cross-section on the Yukawa coupling.

Recently, the NLO QCD corrections to the total cross-section have been computed [10]. They turn out to be important at moderate energies, due to rescattering diagrams, which are generated by the Coulombic gluons exchange between the top quarks near the  $t\bar{t}$  threshold. As a consequence, the total cross-section can be enhanced by a factor 2 with respect to LO whereas, since virtual and soft-gluon radiation are the dominant corrections, the Higgs and top quark energy and angular distributions are hardly changed. However, above threshold these corrections to the total cross-section are small ( $\sim 5\%$  at  $\sqrt{s} = 1$  TeV) and negative, so for the purpose of this analysis they can be safely neglected.

Since the Yukawa coupling is determined from the cross-section measurement, it is straightforward to estimate the expected statistical and some systematic uncertainties on  $g_{t\bar{t}H}$  for a given selection with efficiency  $\epsilon$  and purity  $\rho$ , applied on a data sample corresponding to an integrated luminosity  $L$ :

$$\left( \frac{\Delta g_{t\bar{t}H}}{g_{t\bar{t}H}} \right)_{stat} \simeq (\Delta g_{t\bar{t}H}^2)_{stat} = \frac{1}{S_{stat}(g_{t\bar{t}H}^2)\sqrt{\epsilon\rho L}}, \quad (2.1)$$

$$\left( \frac{\Delta g_{t\bar{t}H}}{g_{t\bar{t}H}} \right)_{syst} \simeq (\Delta g_{t\bar{t}H}^2)_{syst} = \frac{1}{S_{syst}(g_{t\bar{t}H}^2)} \left[ \frac{1-\rho}{\rho} \frac{\Delta\sigma_B^{eff}}{\sigma_B^{eff}} \oplus \frac{1}{\rho} \frac{\Delta L}{L} \oplus \frac{\Delta\epsilon}{\epsilon} \right], \quad (2.2)$$

where  $(\Delta g_{t\bar{t}H}/g_{t\bar{t}H})_{syst}$  accounts for the uncertainties in the effective background cross-

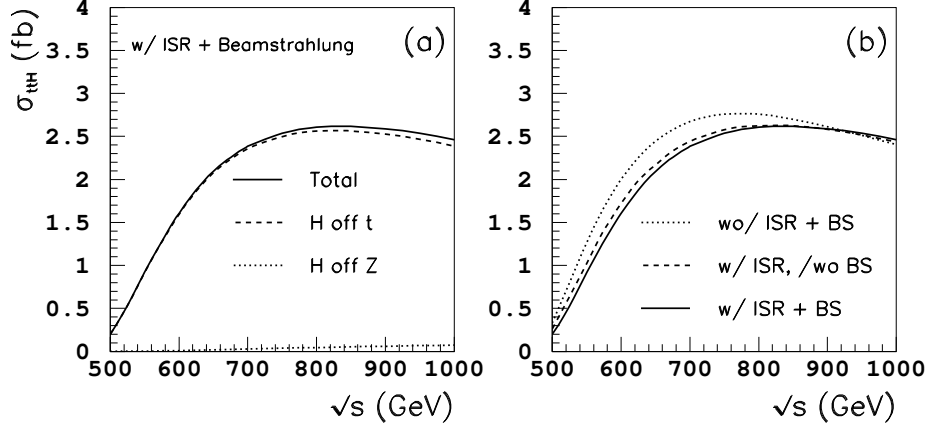


Figure 2: Total cross-section for  $t\bar{t}H$  at lowest order, for  $m_t = 175$  GeV and  $M_H = 120$  GeV, as a function of the center-of-mass energy. In (a) the two contributions:  $H$  off the  $t$  (dashed) and  $H$  off the  $Z$  (dotted) are explicited. The effect of radiative processes in the initial state (initial state radiation and beamstrahlung) on the total cross-section is illustrated in (b).

section (after selection), the integrated luminosity and the selection signal efficiency.  $S_{stat}(g_{ttH}^2)$  and  $S_{syst}(g_{ttH}^2)$  are the so-called “sensitivity factors”, defined as:

$$S_{stat}(g_{ttH}^2) = \frac{1}{\sqrt{\sigma_{ttH}}} \left| \frac{d\sigma_{ttH}}{dg_{ttH}^2} \right|, \quad (2.3)$$

$$S_{syst}(g_{ttH}^2) = \frac{1}{\sigma_{ttH}} \left| \frac{d\sigma_{ttH}}{dg_{ttH}^2} \right|, \quad (2.4)$$

which are a function of  $\sqrt{s}$  for a fixed  $M_H$ .

The sensitivity factors as a function of the center-of-mass energy are shown in Fig. 3a for  $M_H = 120$  GeV. As it can be observed,  $S_{stat}$  reaches a “plateau” for  $\sqrt{s} \geq 700$  GeV, whereas  $S_{syst}$  is essentially independent of  $\sqrt{s}$ . At  $\sqrt{s} = 800$  GeV, the respective values are:  $S_{stat} \simeq 3.09 \text{ fb}^{1/2}$  and  $S_{syst} \simeq 1.92$ . Therefore, assuming an ideal selection ( $\epsilon = 100\%$  and  $\rho = 100\%$ ), a statistical precision of around 1% could be achieved in  $g_{ttH}$  for  $\sqrt{s} \geq 700$  GeV and  $L = 1000 \text{ fb}^{-1}$ . In a more realistic situation of  $\epsilon = 5\%$  and  $\rho = 50\%$ , the statistical uncertainty would be  $\simeq 6.5\%$ , whereas the systematic uncertainty would be dominated by the uncertainty in the background normalization, if one assumed that both the signal selection efficiency and integrated luminosity can be known at the 1% level or better.

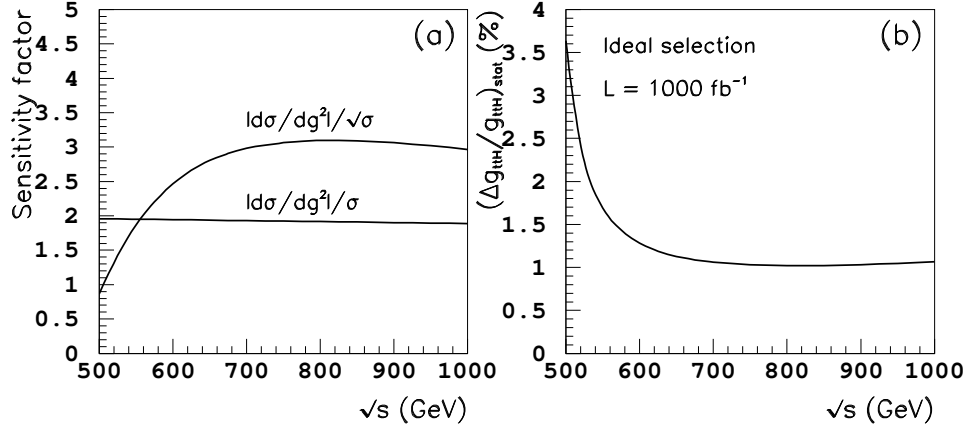


Figure 3: Sensitivity of the total cross-section on the top-Higgs Yukawa coupling as a function of the center-of-mass energy for  $M_H = 120$  GeV and including radiative effects: (a) “sensitivity factors”, (b) statistical uncertainty for an ideal selection assuming an integrated luminosity of  $1000 \text{ fb}^{-1}$ .

### 3 Simulation Aspects

In order to simulate the signal and the  $t\bar{t}Z$  background, we have written a Monte Carlo event generator by using the squared matrix element as computed by the program MADGRAPH [11] and the HELAS [12] subroutines. The top and Higgs masses are assumed to be  $m_t = 175$  GeV and  $M_H = 120$  GeV, respectively. The top width is computed including NLO QCD corrections. Tops are generated off-shell by including the corresponding Breit-Wigner distributions in the differential cross-section. The total cross-section and differential distributions are found to be in good agreement with the calculation in [8]. The rest of backgrounds have been generated with PYTHIA [13]. Interferences between signal and backgrounds have been neglected. The event samples have been generated at  $\sqrt{s} = 800$  GeV, including initial state radiation and beamstrahlung. Initial state radiation has been considered in the structure function approach and beamstrahlung has been generated with the aid of the CIRCE program [14]. Fragmentation, hadronization and particle decays are handled by JETSET [13], with parameters tuned to LEP2 data.

#### 3.1 Detector Simulation

Once the events have been generated, they are processed through a fast simulation [15] of the response of a detector for the TESLA linear collider. The detector components, which are assumed to be:

- a vertex detector,

- a tracker system with main tracker, forward tracker and forward muon tracker,
- an electromagnetic calorimeter,
- a hadronic calorimeter and
- a luminosity detector,

are implemented according to the TESLA Conceptual Design Report [16].

This fast detector simulation provides a flexible tool since its performance characteristics can be varied within a wide range. The calorimeter response is treated in a realistic way using a parametrization of the electromagnetic and hadronic shower deposits obtained from a full GEANT simulation [17] and including a cluster finding algorithm. Pattern recognition is emulated by means of a complete cross-reference table between generated particles and detector response. The output of the program consists in a list of reconstructed objects: electrons, gammas, muons, charged and neutral hadrons and unresolved calorimeter clusters, as a result of an idealized Energy Flow algorithm incorporating track-cluster matching.

### 3.2 B-tagging

Jets coming from  $b$  and  $c$ -quark decays are tagged based on the non-zero lifetime of these quarks, using the Vertex Detector (VDET). In this study we have assumed the performance of a CCD VDET in a 1 cm radius beampipe.

In order to look for this lifetime signal, we have chosen to use the 3D impact parameter (IP) of each charged track (distance of closest approach between the track and the  $b$  production point). Since the statistical resolution of the IP varies strongly from one track to another, we use the estimated statistical significance of the measured IP to define our tag. The b-tagging algorithm is kept simple so that the success of the analysis does not depend on detector details. More efficient algorithms can be developed by making use of multivariate techniques, such as Neural Networks.

In Fig. 4, the IP significance distributions for different  $Z$  hadronic decays are compared. The lifetime signature can be clearly seen for  $Z \rightarrow b\bar{b}$  in the positive tail.

We will use the IP significance distribution for non-lifetime tracks (those originated from  $Z \rightarrow u\bar{u}, d\bar{d}, s\bar{s}$ ) to define, for each track, a probability “to be consistent with being originated from the primary vertex”. This information can then be combined to get also a probability per jet or per event [18].

In order to test the performance of such b-tagging, we have estimated its efficiency and purity for a given cut in the jet probability. To do so, the Monte Carlo generated quarks are assigned to the reconstructed jets by a matching algorithm which associates those quark-jet pairs with minimum invariant mass, starting from the most energetic quark. Now, an efficiency  $\epsilon_b$  and purity  $\rho_b$  can be defined as:

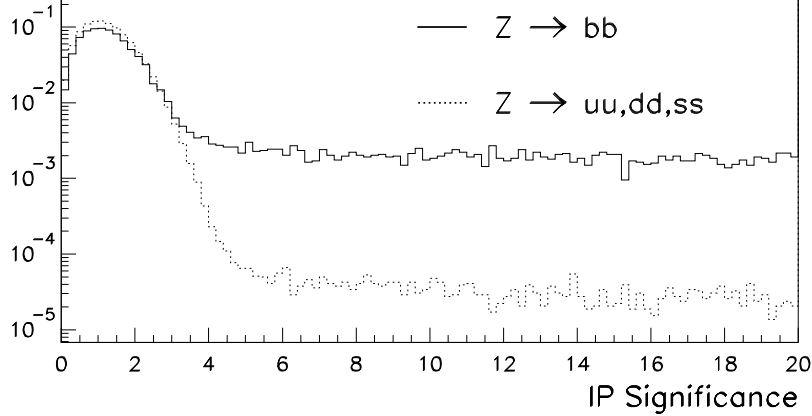


Figure 4: Track 3D impact parameter significance for  $Z$  hadronic events at  $\sqrt{s}=100$  GeV.

$$\epsilon_b = \frac{n_{b,corr}}{n_b}, \quad \text{and} \quad \rho_b = \frac{n_{b,corr}}{n_{b,tag}}$$

where  $n_{b,corr}$  is the number of b-jets correctly tagged,  $n_{b,tag}$  is the total number of tagged b-jets, and  $n_b$  is the actual number of b-jets in the event. In the way the purity is defined here, it measures the misidentification probability of jets in a given process.

The b-tagging efficiencies and purities shown in Fig. 5 as a function of the jet probability cut, correspond to a sample of signal events where the  $W$  leptonic decays have been switched off and the Higgs has been forced to decay into  $b\bar{b}$  ( $t\bar{t}H \rightarrow q\bar{q}q\bar{q}b\bar{b}b\bar{b}$ ). It should be noted that, due to the high multiplicity of such events, the probability that the jet clustering algorithm assigns “lifetime tracks” (coming from the b-jets) to a light-quark ( $uds$ ) jet is large. This leads to rather low values of the b-tagging efficiency such as  $\epsilon_b \sim 80\%$  for a purity of  $\rho_b \sim 60\%$ . In order to quantify the performance degradation of the b-tagging as the event multiplicity increases, this algorithm has been tested with  $ZZ$  events, where one of the  $Z$  bosons has been forced to decay into  $b$  quarks and the other into light-quarks. The achieved b-tagging efficiency in this case is  $\epsilon_b \sim 80\%$  for a purity of  $\rho_b \sim 80\%$ .

Given the low  $\epsilon_b$  values for  $t\bar{t}H$  events, the efficiency to tag correctly the four b-jets of a signal event by fixing a probability cut will be in general very small. In order not to reduce drastically the signal efficiency, we will not use the number of found b-jets for a certain lifetime probability as a selection cut. Instead, for every event, we will define as b-jets those four with the lowest probability (to originate from the primary vertex).

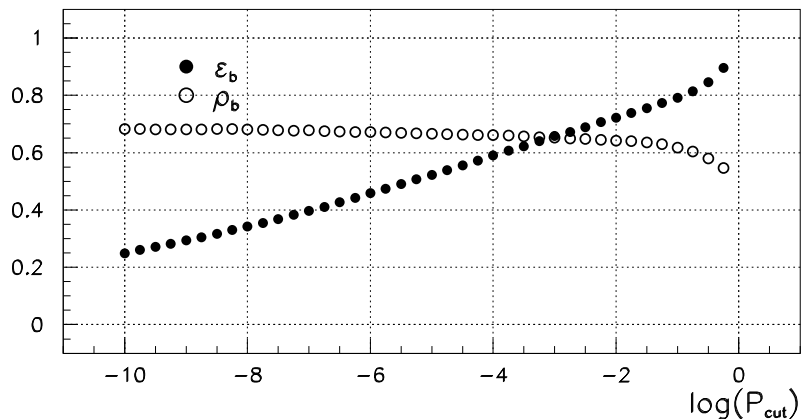


Figure 5: b-tagging efficiency and purity for  $t\bar{t}H \rightarrow q\bar{q}q\bar{q}b\bar{b}b\bar{b}$  events as a function of the lifetime probability cut.

Applied to purely hadronic signal events, for example, this algorithm will tag the four correct b-jets in  $\sim 37\%$  of the cases, and at least three of them in  $\sim 88\%$  of the cases.

## 4 Experimental Analysis

The experimental analysis is performed assuming a total integrated luminosity of  $1000 \text{ fb}^{-1}$ , which can be collected in around 3 years of running at  $\mathcal{L} = 10^{34} \text{ cm}^{-2}\text{s}^{-1}$ .

Both semileptonic and fully hadronic decay channels have been considered. In spite of the apparently clean signature of both channels ( $\geq 6$  jets in the final state, out of which  $\geq 4$  are b-jets, multi-jet invariant mass constraints, etc), the measurement has many difficulties, among which:

- tiny signal ( $\simeq 2.6 \text{ fb}$ ) in front of backgrounds about 3 orders of magnitude larger: in Table 1, the total cross-section for the signal and different backgrounds considered is listed together with the number of generated events.
- limitations of jet-clustering algorithms in properly reconstructing multi-jets in the final state due to hard gluon radiation, jet mixing, etc,
- degradation of b-tagging performance due to hard gluon radiation and jet mixing.

Due to the extremely small signal-to-background (S/B) ratio, the philosophy of the analysis in both decay channels will be to start by applying a standard cuts preselection



Process	$\sigma$ (fb)	Generated events
$t\bar{t}H$	2.57	100k
$q\bar{q}$ (5 flav.)	1557.7	1M
$t\bar{t}$	303.08	1M
$t\bar{t}Z$	4.57	100k
$W^+W^-$	4402.7	3.8M
$ZZ$	308.9	300k
$HZ$ ( $Z \rightarrow t\bar{t}$ )	24.8	100k

Table 1: Total cross-section for signal and the different backgrounds considered at  $\sqrt{s} = 800$  GeV. Initial state radiation and beamstrahlung have been included. Also listed is the number of generated events for every process.

in order to remove as much background as possible while keeping a high efficiency for the signal. Then, in order to further improve the statistical sensitivity, a multivariate analysis will be performed. At this stage our problem will be how to make an optimal use of the statistical information from a set of  $N$  distributions discriminating between signal and background. It can be proven [19] that it is possible to make an optimal projection from this input  $N$ -dimensional space to a 1-dimensional space<sup>1</sup>:

- a) without loss of sensitivity on the classes proportions and
- b) with a probabilistic interpretation (in terms of the a-posteriori Bayesian probability of being of signal type).

This projection can be performed by using Neural Network (NN) techniques, which have become increasingly popular in High Energy Physics in the last few years.

Even after selection, a S/B ratio much larger than 1 can only be obtained at the expense of a rather low signal efficiency. We have considered that the uncertainty on the background normalization after selection is going to be the dominant contribution to the systematic error. The main concern is how well parton shower can reproduce the tails in the distributions for those non-interfering background processes. In order to be just limited by that, it is important to have available event generators with 8 fermions in the final state, thus properly accounting for all interfering backgrounds. The main background process after selection is  $t\bar{t}$ . Therefore, theoretical calculations up to  $\mathcal{O}(\alpha_s^2)$  would be needed by the time this measurement is performed.

For a given systematic uncertainty in the background normalization, it is possible to adjust the selection signal efficiency in order to optimize the total uncertainty in the

---

<sup>1</sup>In the general case of  $m$  existing classes to be discriminated, the optimal projection is performed in a space  $(m - 1)$ -dimensional. In our problem, all backgrounds are considered inclusively and  $m = 2$ , thus the optimal projection being 1-dimensional.

Yukawa coupling. We have set as a goal a 5% systematic uncertainty in the background normalization in order not to dominate the measurement. Then, we have optimized the selection assuming this uncertainty.

#### 4.1 Semileptonic Channel

The semileptonic decay channel, with a branching ratio of 43.9%, constitutes the golden channel in terms of high statistics and clean signature as compared to the fully hadronic decay channel, where 8 jets have to be reconstructed in the final state. The final state is:

$$e^+e^- \rightarrow t\bar{t}H \rightarrow q\bar{q}b\ell^\pm\nu_\ell\bar{b}\bar{b},$$

the experimental signature being then: 4 b-jets + 2 light-quark jets +  $\ell^\pm + E_{miss}$ . Hence, the high  $p_T$  and isolated lepton can be used for triggering purposes and might provide clear separation in the offline selection as well. The four-momentum imbalance due to the neutrino presence will also represent a discriminant variable as long as the final detector has a good hermeticity. Finally, the high content in b-jets will also be exploited as a powerful discriminant variable by using the vertex detector.

As already stated, the philosophy of the selection has been to start with a series of preselection cuts addressed to remove as much background events as possible while keeping high efficiency for the signal. The preselection variables are compared for signal and background in Figs. 8 and 9, along with the cuts applied. The selected events are required to have a visible mass larger than 500 GeV but lower than 800 GeV, more than 60 energy flow (EF) objects reconstructed and at least 6 jets reconstructed with the JADE [20] jet-clustering algorithm for a resolution parameter  $y_{cut} = 10^{-3}$ . Then a series of cuts on topological variables such as the thrust and the normalized Fox Wolfram moments of the event are applied. These cuts are mainly addressed to drastically reduce the contamination of high cross-section backgrounds such as  $W^+W^-$  or radiative  $q\bar{q}$ , which tend to be much less spherical than signal events (due to the boost) and have a large value for these variables (see Fig. 9). Also useful are the so-called high and low jet masses of the event,  $PmH$  and  $PmL$ , respectively. The event is divided in two hemispheres and particles are assigned to either hemisphere in order to minimize the quadratic sum of the two hemispheres invariant masses. For processes with two resonances (such as  $W^+W^-$  or  $ZH$ ), these distributions tend to show resonant structures around the true invariant masses.

At this stage, and in order to reconstruct the  $t\bar{t}H$  semileptonic decay signature, an energetic and isolated lepton has to be identified. This lepton candidate has been chosen as the charged track which maximizes  $E_\ell(1 - \cos\theta_{\ell j})$ , where  $E_\ell$  is the track energy and  $\theta_{\ell j}$  the angle of such track with the closest of the 6 jets to which the remaining EF objects have been forced by using JADE. The efficiency of such algorithm to find the correct lepton (the one from the  $W$  decay) for  $t\bar{t}H$  semileptonic events has been determined to be  $\sim 98\%$ .

Once the event has been clustered into 6 jets plus 1 lepton and after rejecting those events having jets with less than 3 EF objects, a probability to contain no-lifetime is assigned to each jet as described in Sect. 3.2. This allows us to build a powerful variable which reflects the lifetime content of the event by adding up the probabilities of the four most b-like jets (those with lower non-lifetime probability).

In Table 2 the preselection efficiencies for the signal and the different backgrounds are displayed. The situation is such that the overall effective cross-section for the background is 17.60 fb, while for the signal is only 0.61 fb. This translates into such a poor sample purity ( $\rho \sim 3.3\%$ ), that any uncertainty in the background normalization completely erases any significance in the signal.

Process	$\epsilon$ (%)	$\sigma_{eff}$ (fb)
$t\bar{t}H \rightarrow 6q\ell\nu$	54.08	0.61
$t\bar{t}H \rightarrow 8q + 4q\ell\nu\ell\nu$	18.80	0.27
$q\bar{q}$ (5 flav.)	0.102	1.18
$t\bar{t}$	3.621	10.97
$t\bar{t}Z$	21.08	0.96
$W^+W^-$	0.092	4.05
$ZZ$	0.053	0.16
<i>Total Bckg</i>		17.59

Table 2: Semileptonic channel preselection efficiencies and effective cross-sections.

However, there are several variables which, after the preselection, still have some discriminating power. We will use a NN in order to project in an optimal way this N-dimensional information into a 1-dimensional variable.

Nine variables showing high discrimination at the preselection level (see Fig. 10) have been chosen to train a NN to separate the signal from the background. Three of these variables use the information of the leptonic decay of one of the  $W$  bosons (lepton energy, angle between lepton and closest jet and invariant mass between the lepton and the missing momentum), two use the b-jets content of the event (global no-lifetime probability for the event and sum of the no-lifetime probabilities of the four most b-like jets) and four more topological variables (thrust, aplanarity, number of jets clusterized with JADE for  $y_{cut} = 10^{-3}$  and the total visible mass).

After training the NN, the weights distribution for the different neurons allows to determine the discriminant power of each of the 9 input variables (see Table 3). It can be seen that the most discriminating variables are those containing b-tagging information, followed by the identified lepton related variables.

The NN output distributions for the signal and the different backgrounds are compared in Fig. 11. The histograms have been normalized to the same integrated luminosity (1000

Variable	Discriminant Power (%)
$M_{\text{vis}}$	7.2
$N_{\text{jets}}(\text{JADE})$	9.0
$\sum_{i=1,4} P_{\text{btag}}^{\text{jet } i}$	21.4
$\text{Log}(P_{\text{btag}}^{\text{evt}})$	14.4
Thrust	8.5
Aplanarity	7.8
$E_{\ell}$	11.8
$M_{\ell\nu}$	10.8
$\cos\theta_{\ell j}$	9.1

Table 3: Discriminant power of each of the 9 input variables of the semileptonic selection Neural Network.

$\text{fb}^{-1}$ ) to show how, even after having used the information in the 9 variables, the S/B ratio is smaller than one in all the bins.

Applying a cut in the NN output variable allows us to perform an optimal test of decision. A measurement of the  $t\bar{t}H$  cross-section, and hence of the top Yukawa coupling, can then be done assuming the knowledge of the expected number of background events. However, is necessary to take into account the systematic uncertainty in the background normalization which, as already mentioned in Sect. 4, has been assumed here to be at the 5% level.

In Fig. 6 the evolution of both the statistical and systematic uncertainties (as defined above) is plotted as the cut in the NN output is varied. Actually, the horizontal scale is not directly the NN output, but the a-posteriori Bayesian probability of being of signal-type for the expected proportions of signal and background, which can be computed as a function of the NN output. It can be seen how, by cutting harder on the NN output, the systematic error coming from the background normalization can be kept under control since a higher sample purity is achieved. The optimal cut is found within the plateau in the total error for the minimum possible systematic uncertainty.

In Table 4, the statistical and systematic uncertainties are compared in different steps, illustrating the usefulness of the multivariate analysis. As already mentioned, the sample purity after preselection is so poor that, not only the statistical error degrades because of statistical fluctuations in the background, but the systematic error (see Eq. 2.2) introduced as a result of 5% uncertainty in the background normalization leads effectively to the absence of a measurement. The situation is dramatically improved when using a multivariate analysis and the top-Higgs Yukawa coupling is determined from a fit to the output neuron distribution. The systematic uncertainty can be further controlled (at the expense of slightly increasing the statistical uncertainty) by choosing a suitable cut in the NN output distribution.

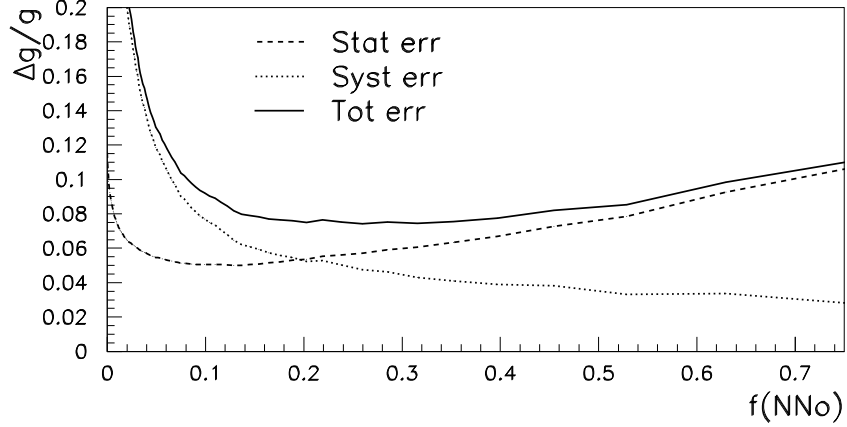


Figure 6: Evolution of the error in the top Yukawa coupling as a function of the NN output cut (semileptonic channel).

	$\epsilon$ (%)	S/B	Stat. error (%)	Syst. error (%)	Total error (%)
After Preselection	54.1	0.03	11.5	63.1	64.1
Fit to NNSEL (50 bins)	"	"	4.4	9.1	10.1
NNSEL>0.9 (optimal cut)	27.1	0.51	5.1	3.8	6.3

Table 4: Statistical and systematic uncertainties in the top-Higgs Yukawa coupling from the semileptonic channel. An integrated luminosity of  $1000 \text{ fb}^{-1}$  has been assumed.

## 4.2 Hadronic Channel

The fully hadronic decay channel, with a branching ratio of 45.6%, benefits from the high statistics but is the most difficult one in terms of signal to background discrimination, experimental reconstruction and the one potentially more affected by systematic uncertainties. The final state is:

$$e^+e^- \rightarrow t\bar{t}H \rightarrow q\bar{q}b\,q\bar{q}\bar{b}\,b\bar{b},$$

the experimental signature being quite challenging: 8 jets in the final state, out of which 4 are b-jets. This imposes quite stringent requirements in the vertex detector. Due to limitations in the jet clustering algorithms, the ability to properly reconstruct 8 jets is not dominated by the detector performance. In this sense, this channel does not impose strict requirements for what the tracker momentum resolution and calorimeter energy resolution and granularity is concerned.

Potential backgrounds are genuine multi-jet processes like  $t\bar{t}$  and  $t\bar{t}Z$ . In fact, the large cross-section of  $t\bar{t}$ , together with hard gluon emission easily emulating 8 jets make of this process the most important background after selection. Of particular concern is  $t\bar{t}g^*$ , with the gluon splitting into a  $b\bar{b}$  pair, since it easily emulates 4 b-jets in the final state, even though the invariant mass of the  $b\bar{b}$  pair from the gluon splitting peaks at low values. Since the assumed Higgs mass is relatively close to the  $Z$  mass,  $t\bar{t}Z$  constitutes an almost irreducible background. The main reason is that the invariant mass resolution of the  $b\bar{b}$  system becomes seriously degraded due to particle mixing between jets in such a populated environment and to energy losses in neutrino emission from the B-meson cascade decays. On the other hand and again due to the large cross-section and limitations in the b-tagging in such a busy environment, hadronic final states such as  $W^+W^- \rightarrow q_1\bar{q}_2q_3\bar{q}_4g^*$ , where the gluon splits into a  $b\bar{b}$  pair will lead to the necessity of a stronger selection and therefore reduced statistical sensitivity on the Yukawa coupling.

Like for the semileptonic channel, a standard cuts preselection is applied in order to remove as much background as possible before the multivariate analysis. The selected events are required to have a visible mass in excess of  $70\%\sqrt{s}$  (that is 560 GeV), more than 120 EF objects reconstructed and at least 7 jets reconstructed with the JADE algorithm for a resolution parameter  $y_{cut} = 10^{-3}$ . Then the event is forced to have exactly 8 jets reconstructed by using JADE. Further preselection cuts require a minimum of 2 EF objects per jet, a minimum di-jet invariant mass of 20 GeV and the thrust larger to 0.85. The preselection variables are compared for signal and background in Fig. 12, along with the cuts applied. The preselection efficiencies and effective cross-section for the different processes considered are listed in Table 5.

Process	$\epsilon$ (%)	$\sigma_{eff}$ (fb)
$t\bar{t}H \rightarrow 8q$	77.06	0.90
$t\bar{t}H \rightarrow 6q\ell\nu + 4q\ell\nu\ell\nu$	9.63	0.14
$q\bar{q}$ (5 flav.)	0.378	4.38
$t\bar{t}$	5.02	15.22
$t\bar{t}Z$	27.35	1.25
$W^+W^-$	0.185	8.14
$ZZ$	0.139	0.43
<i>Total Bckg</i>		29.55

Table 5: Hadronic channel preselection efficiencies and effective cross-sections.

After preselection, the efficiency for signal is reduced to 77% and the sample purity is only  $\simeq 3.0\%$ .

Note the high remaining cross-section for  $q\bar{q}$  and  $W^+W^-$  despite the cuts applied, e.g. in minimum di-jet invariant mass. The main responsible is hard gluon radiation. In

Table 6, the average number of gluons with  $P_g > 20$  GeV/c, average gluon momentum and angle of the gluon with respect to the parent quark are listed for both processes, before and after preselection. Indeed, multi-gluon radiation (as simulated by parton shower) leads to genuine 8-jet final state even for processes like  $q\bar{q}$  (5 flav.)/ $W^+W^-$  with only 2/4 initial partons. Owing to the large cross-section of these processes, they constitute non-negligible backgrounds which have to be taken into account in any “realistic simulation”.

Process	$\langle N_g \rangle$	$\langle P_g \rangle$ (GeV/c)	$\langle \theta_{gq} \rangle$ (deg.)
$q\bar{q}$ (5 flav.)	4.2(6.9)	64.6(50.0)	16.0(44.4)
$W^+W^-$	3.8(4.0)	61.6(45.4)	6.3(22.7)

Table 6: Hard gluon ( $P_g > 20$  GeV/c) radiation as predicted by parton shower at  $\sqrt{s} = 800$  GeV before and after (between parenthesis) preselection.

As it can be observed in Fig. 12, the preselection variables after cuts still have discriminating power between signal and background. In order to optimally use these variables, they are further used together with two more variables to train a Preselection Neural Network. The two variables added (shown as the two last variables in Fig. 12) provide information about the lifetime content of the event: the logarithm of the event probability to contain no-lifetime and the difference between the probability of the fourth jet and the first jet (sorted from the most b-like to the least b-like). In Fig. 7 it is shown the Preselection Neural Network output, after training, for both signal and background. No cut is applied in this distribution, but it is rather used as a discriminant variable.

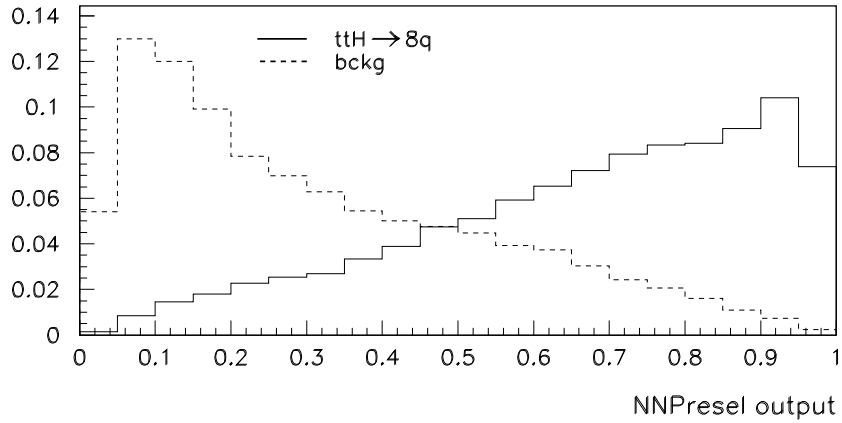


Figure 7: Hadronic preselection Neural Network output. Signal (solid) and background (dashed) have been normalized to the same number of events.

There are 10 more variables which are discriminating between signal and background (see Fig. 13). Most of them are variables about the global event topology:

- Njets(LUCLUS, dcut=6.5 GeV): number of jets found with the LUCLUS [21] jet-clustering algorithm for a distance measure of 6.5 GeV;
- PmH and PmL: high and low jet masses of the event, already described;
- Max(Ejet)-Min(Ejet): difference between maximum and minimum jet energy;
- Evis: total visible energy of the event;
- Thrust, Oblateness, Aplanarity,

others contain information about flavor tagging (SumPbtagOrd: sum of the probability to contain no-lifetime for the four most b-like jets) or Higgs mass reconstruction:

- Reco Higgs mass: reconstructed Higgs mass. The 4 most b-like jets are assumed to be the b-jets, which reduces the number of possible jet assignments to 36. The combination which maximizes:

$$\mathcal{P}(m_{i_1 i_2 i_3} - m_t) \times \mathcal{P}(m_{i_4 i_5 i_6} - m_t) \times \mathcal{P}(m_{i_1 i_2} - m_W) \times \mathcal{P}(m_{i_4 i_5} - m_W) \times \mathcal{P}(m_{i_7 i_8} - m_H),$$

is selected. In the above expression  $\mathcal{P}$  are the probability density functions for the correct jet pairing and  $m_{ij}$  ( $m_{ijk}$ ) is the invariant mass between jets  $i$  and  $j$  ( $i$ ,  $j$  and  $k$ ).

These variables, together with the Preselection Neural Network output distribution are used to train a Selection Neural Network. After training, it is found that the most discriminating variables are the Preselection Neural Network output, reconstructed Higgs mass, thrust and aplanarity (see Table 7). The output neuron distribution is compared for signal and background in Fig. 14.

As for the semileptonic decay channel, in Table 8 the statistical and systematic uncertainty (from 5% background normalization uncertainty only) on the top-Higgs Yukawa coupling are compared in different steps.



Variable	Discriminant Power (%)
$E_{\text{vis}}$	5.9
$\max(E^{\text{jet}}) - \min(E^{\text{jet}})$	7.6
$N_{\text{jets}}(\text{LUCLUS})$	6.9
Thrust	13.3
Aplanarity	11.5
Oblateness	5.4
High jet mass	7.3
Low jet mass	8.2
$\sum_{i=1,4} P_{\text{btag}}^{\text{jet } i}$	6.5
$M_{\text{H}}^{\text{reco}}$	11.7
$O_{\text{NN}}^{\text{presel}}$	15.7

Table 7: Discriminant power of each of the 11 input variables of the hadronic selection Neural Network.

	$\epsilon$ (%)	S/B	Stat. error (%)	Syst. error (%)	Total error (%)
After Preselection	77.1	0.03	9.8	83.5	83.5
Fit to NNSel (50 bins)	"	"	4.2	13.7	14.3
NNSel>0.95 (optimal cut)	8.5	0.90	7.3	3.0	7.9

Table 8: Statistical and systematic uncertainties in the top-Higgs Yukawa coupling from the fully hadronic channel. An integrated luminosity of  $1000 \text{ fb}^{-1}$  has been assumed.

## 5 Conclusions

The reaction  $e^+e^- \rightarrow t\bar{t}H$  allows a direct determination of the top-Higgs Yukawa coupling through its total cross-section measurement. We have studied the feasibility of this measurement for  $M_H = 120$  GeV in a future  $e^+e^-$  linear collider operating at  $\sqrt{s} = 800$  GeV and assuming  $1000 \text{ fb}^{-1}$  of integrated luminosity.

The analysis has been performed for both hadronic and semileptonic decay channels, which constitute almost 90% of all decays. For both of them, several sources of background have been considered, including not only the interfering ones like  $t\bar{t}Z$  (although interferences have been neglected) but also those non-interfering like  $q\bar{q}$  or  $W^+W^-$  but which have huge cross-sections as compared to that of the signal.

In both cases, a set of variables with high discriminating power has been chosen to perform a multivariate analysis in order to use their N-dimensional information in a way as optimal as possible. For the two studied channels, topological variables have been used as well as some others containing b-tagging information.

Our final results show the statistical uncertainties that can be achieved in each channel for an integrated luminosity of  $1000 \text{ fb}^{-1}$ . We have estimated as well the systematic uncertainty that would be associated to a 5% uncertainty in the overall background normalization (even though the main remaining background is  $t\bar{t}$ ) as a way to quantify the importance of an improvement in such theoretical uncertainty by the time the measurement might be performed.

As a final result we can quote the combination of the two channels considering the systematic uncertainty fully correlated between them, which leads to a total uncertainty in the top-Higgs Yukawa coupling of  $\simeq 5.5\%$ . The statistical uncertainty only would be  $\simeq 4.2\%$ .

## 6 Acknowledgements

We are grateful to M. Martínez and P.M. Zerwas for valuable discussions.

## References

- [1] J. Ellis, M.K. Gaillard, D.V. Nanopoulos, Nucl. Phys. **B106** (1976) 292.  
J.D. Bjorken, Proc. SLAC Summer Institute, 1976.  
B. Ioffe, V. Khoze, Sov. J. Part. Nucl. Phys. **9** (1978) 50.  
B.W. Lee, C. Quigg, H.B. Thatcher, Phys. Rev. **D16** (1977) 1519.
- [2] D.R.T. Jones, S.T. Petcov, Phys. Lett. **84B** (1979) 440.  
R.N. Cahn, S. Dawson, Phys. Lett. **136B** (1984) 196.  
G. Altarelli, B. Mele, F. Pitolli, Nucl. Phys. **B287** (1987) 205.
- [3] M. Martínez *et al.*, in *Conference on Physics and Experiments with Linear Colliders, Morioka-Appi, Japan, September 1995*.  
K. Fujii, in contribution by P. Igo-Kemenes, in *Conference on Physics and Experiments with Linear Colliders, Waikoloa, Hawaii, USA, 1993*.
- [4] H. Baer, S. Dawson and L. Reina, hep-ph/9906419, June 1999.  
M. Sachwitz, S. Shichanin and H. Schreiber (work in progress as reported in LCWS99).
- [5] LEPEWWG, EP Preprint Summer 98 CERN-EP/99-15.
- [6] ALEPH 99-081 CONF 99-052  
DELPHI 99-142 CONF 327  
L3 Note 2442  
OPAL Technical Note TN-614.
- [7] M. Jezabek and J.H. Kühn, Phys. Lett. **B316** (1993) 360.
- [8] A. Djouadi, J. Kalinowski and P. Zerwas, Z. Phys. **C54** (1992) 255.
- [9] E. Accomando *et al.*, Phys. Rep. **299** (1998) 1.
- [10] S. Dittmaier, M. Kramer, Y. Liao, M. Spira and P. Zerwas, Phys. Lett. **B44** (1998) 383.  
S. Dawson and L. Reina, Phys. Rev. **D59** (1999) 054012.
- [11] MADGRAPH, by T. Stelzer and W.F. Long, Comp. Phys. Com. **81** (1994) 357.
- [12] HELAS, by H. Murayama, I. Watanabe and K. Hagiwara, KEK-91-11 (1992).
- [13] T. Sjöstrand, Comp. Phys. Com. **82** (1994) 74.
- [14] T. Ohl, *Beam Spectra for Simulating Linear Collider Physics*, hep-ph/9607454-rev, July 1996 (expanded September 1996).

- [15] M. Pohl and H.J. Schreiber, *SIMDET-Version 3, A Parametric Monte Carlo for a TESLA Detector*, DESY Preprint DESY 99-01, January 1999.
- [16] R. Brinkmann, G. Materlik, J. Rossbach and A. Wagner Eds., Conceptual Design of a 500 GeV  $e^+e^-$  Linear Collider with Integrated X-ray Laser Facility, DESY 1997-048 and ECFA 1997-182 (1997).
- [17] T. Behnke, G. Blair, K. Möning and M. Pohl, *BRAMHS-Version 1.00, a Monte Carlo Program for a Detector at a 800 GeV Linear Collider*, November 8 , 1998, <http://www.hep.ph.rhbnc.ac.uk/~blair/detsim/bramhs.html>.
- [18] D. Brown and M. Frank, *Tagging  $b$  hadrons using track impact parameters*, ALEPH 92-135 PHYSIC 92-124.
- [19] Ll. Garrido, S. Gómez, A. Juste and V. Gaitan, *Optimal projection to estimate the proportions of the different subsamples in a given mixture sample*, Comp. Phys. Com. **104** (1997) 37.
- [20] W. Bartel *et al.* (JADE Collaboration), Z. Phys. **C33** (1986) 23.
- [21] T. Sjöstrand, Comp. Phys. Com. **22** (1983) 227.

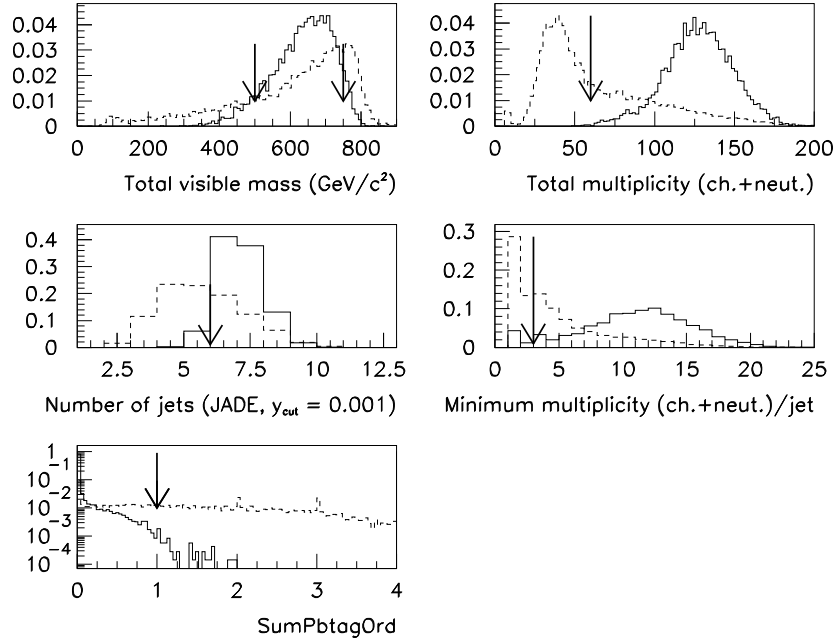


Figure 8: Preselection variables for the semileptonic channel (I). Signal (solid) and background (dashed) have been normalized to the same number of events. The background histograms have been built by adding all the different backgrounds contributions weighted according to their relative cross-sections.

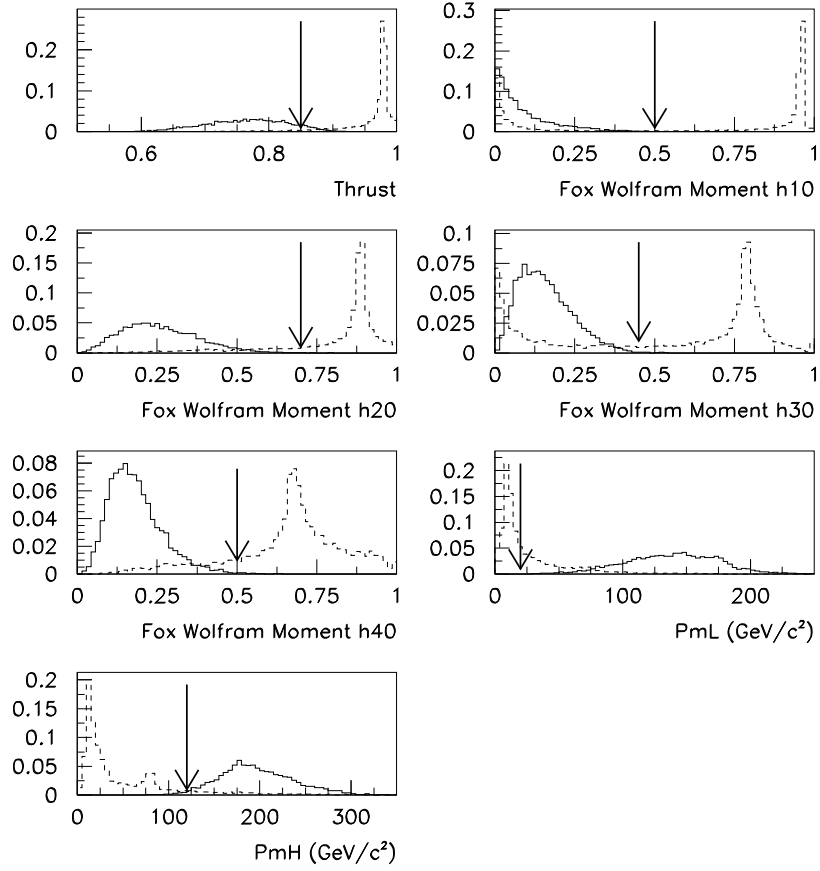


Figure 9: Preselection variables for the semileptonic channel (II). Signal (solid) and background (dashed) have been normalized to the same number of events. The background histograms have been built by adding only the  $W^+W^-$  and  $q\bar{q}$  contributions weighted according to their relative cross-sections. In this way the differences between the signal and the most topologically different backgrounds are clearly visualized.

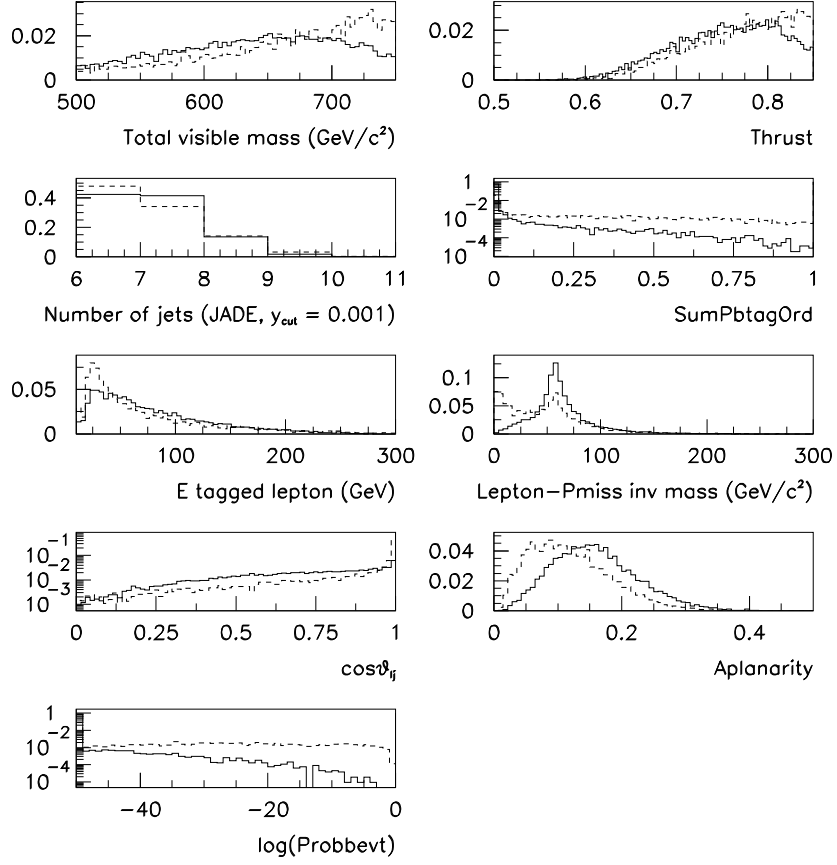


Figure 10: Selection Neural Network variables for the semileptonic channel. Signal (solid) and background (dashed) have been normalized to the same number of events. The background histograms have been built by adding all the different backgrounds contributions weighted according to their relative cross-sections.

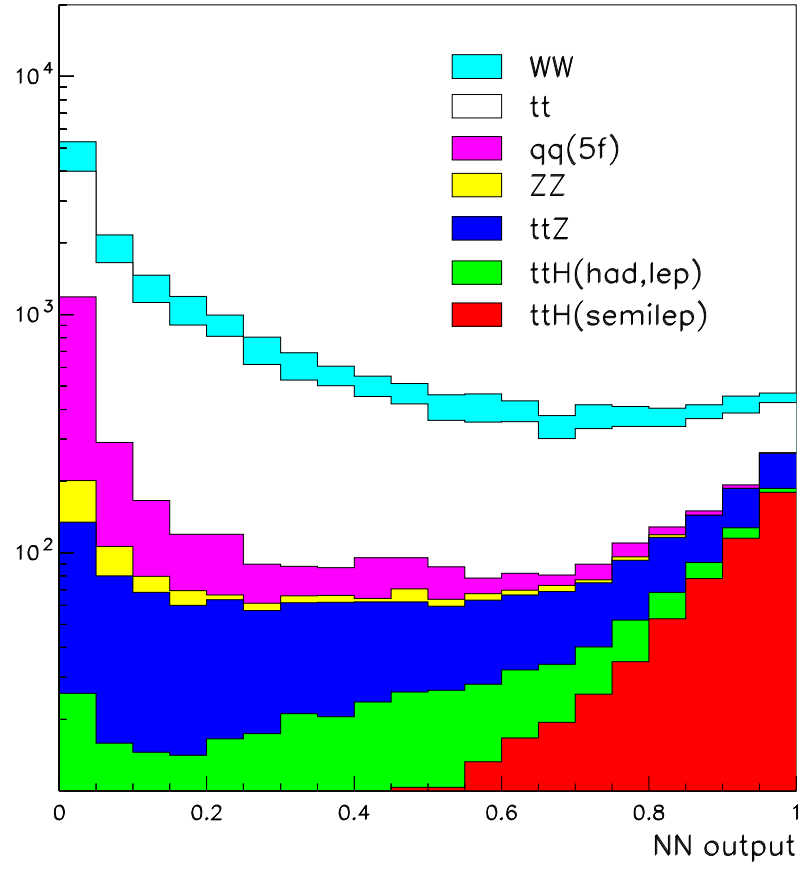


Figure 11: Semileptonic Selection Neural Network output. The different contributions are normalized to the same luminosity ( $1000 \text{ fb}^{-1}$ ).



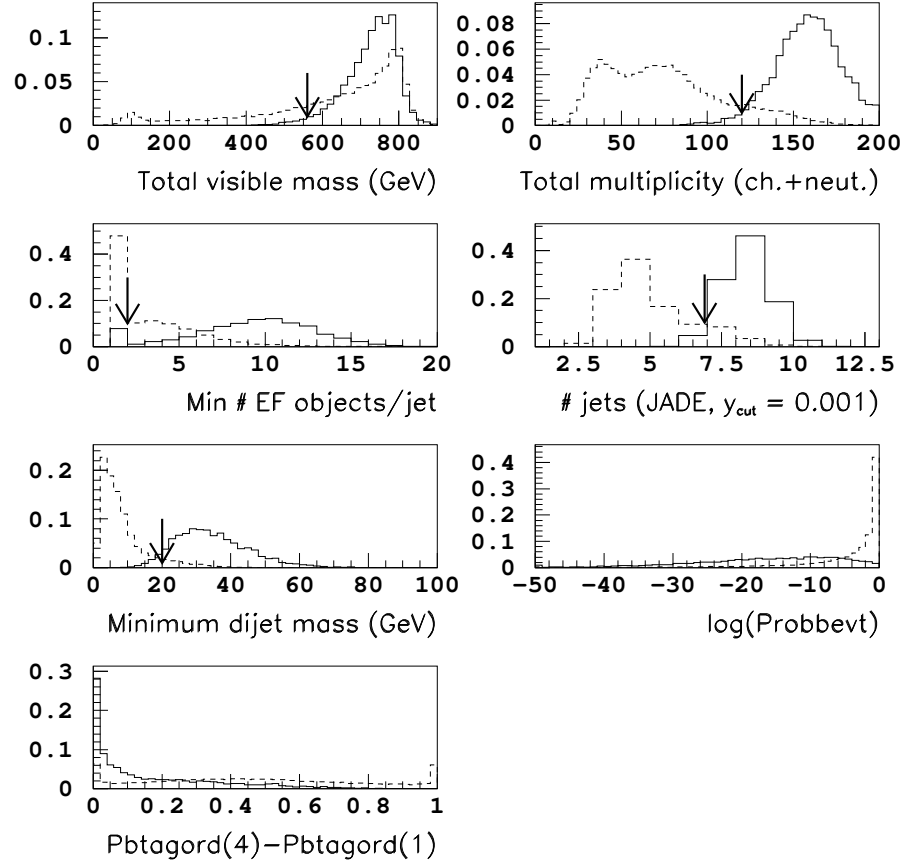


Figure 12: Preselection variables for the hadronic decay channel. Signal (solid) and background (dashed) have been normalized to the same number of events. The background prediction has been computed by adding all the different background contributions weighted according to their relative cross-section.

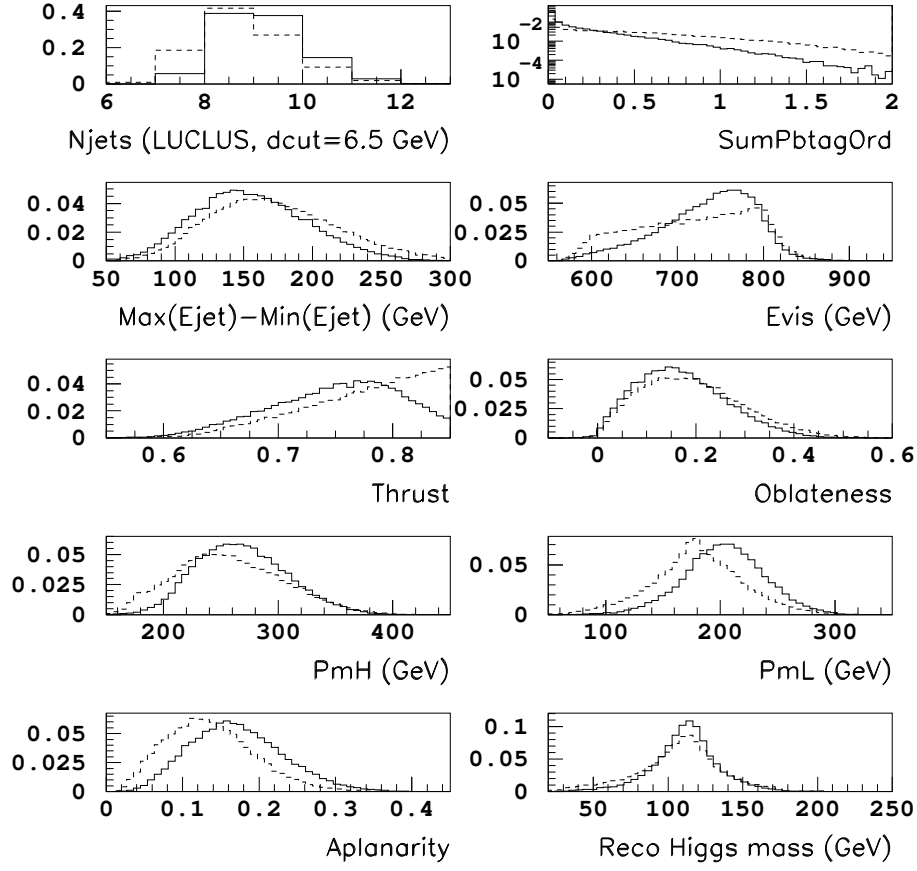


Figure 13: Selection Neural Network variables for the hadronic decay channel. Signal (solid) and background (dashed) have been normalized to the same number of events. The background prediction has been computed by adding all the different background contributions weighted according to their relative cross-section.

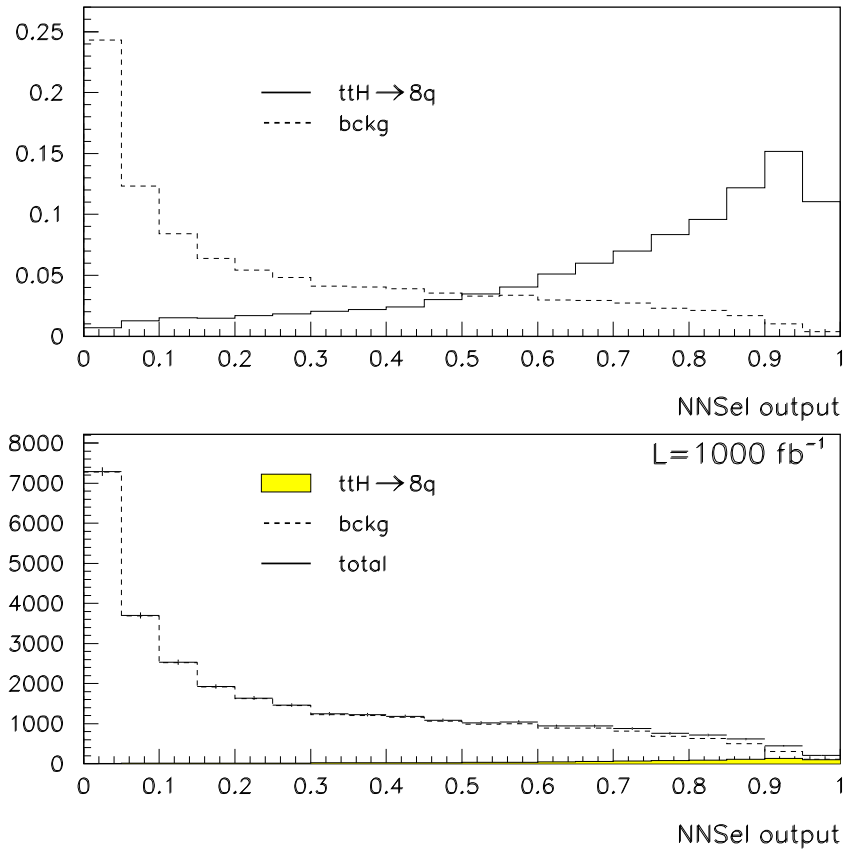


Figure 14: Hadronic selection Neural Network output. Top: Signal (solid) and background (dashed) have been normalized to the same number of events. Bottom: comparison of signal (shaded) and background (dashed) for  $L = 1000 \text{ fb}^{-1}$ .